MOX-Report No. 07/2020

Reactive flow in fractured porous media

Fumagalli, A.; Scotti, A.

MOX, Dipartimento di Matematica
Politecnico di Milano, Via Bonardi 9 - 20133 Milano (Italy)

mox-dmat@polimi.it http://mox.polimi.it

Reactive flow in fractured porous media

Alessio Fumagalli and Anna Scotti

Abstract In this work we present a model reduction procedure to derive a hybrid-dimensional framework for the mathematical modeling of reactive transport in fractured porous media. Fractures are essential pathways in the underground which allow fast circulation of the fluids present in the rock matrix, often characterized by low permeability. However, due to infilling processes fractures may change their hydraulic properties and become barriers for the flow creating impervious blocks. The geometrical as well as the physical properties of the fractures require a special treatment to allow the subsequent numerical discretization to be affordable and accurate. The aim of this work is to introduce a simple yet complete mathematical model to account for such diagenetic effects where chemical reactions will occlude or empty portions of the porous media and, in particular, fractures.

Key words: Reduced modeling, hybrid-dimensional framework, fracture porous media, reactive flow

MSC (2010)**:** 80A32, 76S05, 35Q86

1 Introduction

Fractures play a crucial role in determining fluid flow in a geological system. However, two critical parameters make the modelisation of fractures challenging from

Alessio Fumagalli
Politecnico di Milano,
via Bonardi 9, 20133 Milan, Italy
e-mail: Alessio.Fumagalli@polimi.it

Anna Scotti
Politecnico di Milano,
via Bonardi 9, 20133 Milan, Italy
e-mail: Anna.Scotti@polimi.it

both mathematical and numerical points of view. These are their apertures, which normally are several order of magnitude smaller than any other dimensions in the problem, and their microscopic structure: fractures can be open or filled by porous materials. Fractures thus can behave as highly conductive flow pathways that link distant parts of the geological system and allow for fast circulation of fluid or, on the opposite side, can be clogged preventing the flow and creating impervious parts which are not reachable. A fracture can have a portion of its core partially or fully filled and another portion empty. Such complexity normally creates problems for classical models.

In addition the fluids present in the underground can carry ions of different types that, under certain thermal conditions, might interact and react forming salts that precipitate and attach to the walls of the void spaces of the porous media. This process tends to reduce the void spaces with a direct impact on the flow properties of the system. We will call these salts "precipitate" while the ions are called "solutes". Conversely, if a precipitate is already present and the environmental conditions are such that it can dissolve we will have an increment of the porosity (i.e. void space) and the creation of ions that can be transported by the liquids. Some reference on this subject are: reactive transport on porous media at pore-scale [22, 12, 28] and at macro-scale [25, 14, 1] with experiment comparison [24]. For an micro to macro upscaling procedure see [29, 30].

In presence of fractures the situation is even more complex. The deposition or dissolution reactions can also take place inside the fractures, substantially altering their physical properties and impacting the global flow properties of the geological system. This work aims to introduce a mathematical model to accurately describe this phenomena with the technique of dimensionality reduction. This technique is rather standard in the treatment of problem with thin interfaces and frequently used in problems involving fractures. Single-phase flow [2, 27, 11, 16, 31, 17, 4, 33, 7, 9, 34, 6], two-phase flow [23, 18, 13], passive transport [19, 10, 3], and poro-elasticity [20, 8, 35, 5] are some of the physical problems which have been successfully modeled with this technique.

This work is organised as follow: in Section 2 the mathematical model for flow and reactive transport in a porous media is presented. Section 3 is devoted to the derivation of the reduced model to describe the fracture flow and transport via reduced models. Finally, Section 4 contains the conclusion of this work.

2 Reactive flow

In this section we present the mathematical model which describes the flow in porous media and the transport of several species of ions (solutes). These may react forming a salt and the salt may in turn dissolve forming the ions. We consider two possible reactions: *i)* the precipitation or crystallisation where these solutes form a solid part or *ii)* a dissolution. For simplicity in the exposition, we consider only one precipitate.

The porous media is described by the domain $\Omega \subset \mathbb{R}^n$, for $n = 2,3$. We suppose that the porous media is saturated by a single liquid phase, e.g. water, and the ions are transported by its motion. Finally, the fine scale composition of the porous media is such that a Darcy model at macroscopic scale can be applied. Our presentation is indeed given at the macro-scale. For simplicity, the initial time is assumed to be 0.

2.1 Reactive model

Let us consider several solutes $\{U_i\}_{i=1}^N$ which are transported in the porous media by a liquid phase. As already mentioned, these solutes may react to form a solid part W. The integer N indicates the number of species of ions that are involved in the chemical reactions,which can be written as

$$\sum_{i=1}^{N} \alpha_i^+ U_i \leftrightarrow W + \sum_{i=1}^{N} \alpha_i^- U_i. \tag{1}$$

The terms $\alpha_i^\pm \geq 0$ are the stoichiometric coefficients of the reactions. Each reaction (precipitation and dissolution) is characterized by a reaction constant $\lambda^\pm$, being λ^+ the one associated with the precipitation and λ^- the one associated with the dissolution. We have $\lambda^\pm \geq 0$. We indicate with $\{u_i\}_{i=1}^N$ and w the molar concentration of the species $\{U_i\}_{i=1}^N$ and W, respectively. We have the lower bound $u_i \geq 0$, for all $i = 1,\dots,N$, as well as $w \geq 0$. We can write the net precipitation rate associated with the reaction (1) in the following way

$$r_w(\{u_i\}_{i=1}^N) = \lambda^+ \prod_{i=1}^{N} u_i^{\alpha_i^+} - \lambda^- \prod_{i=1}^{N} u_i^{\alpha_i^-},$$

the first term being the rate of creation of solid part w and the second term the dissolution rate of the solid part in a unit time.

For simplicity, we suppose only one spice of positive ions and one spice of negative ions, meaning $N = 2$. Moreover, we assume electrical equilibrium, *i.e.* number of anions equal to the number of cations, and thus we can have $u_i = u$ for $i = 1,2$. The previously introduced reaction rate can be simplified as

$$r_w(u) = \lambda^+ u^{\alpha^+} - \lambda^- u^{\alpha^-} \quad \text{with} \quad \alpha^\pm = \alpha_1^\pm + \alpha_2^\pm. \tag{2}$$

We consider that the dissolution of w does not depend on the presence of ions u whereas precipitation involves all the ions present. In formula, if we assume that $\alpha_i^- = 0$, for $i = 1,2$, and (2) becomes

$$r_w(u) = \lambda^- \left(\frac{\lambda^+}{\lambda^-} u^{\alpha^+} - 1 \right).$$

Inspired by the previous relation, we can finally write the more abstract reaction rate law that is considered in this work. In a more compact way, we have

$$r_w(u) = \lambda[r(u) - 1],$$

with $\lambda \geq 0$ a coefficient and $r(u) = u^\zeta$, with ζ a positive integer. The previous models suffer of an inconsistency, in fact they do not not vanish in the limit case of $w = 0$ and might create negative values of the quantities involved. To overcome this problem, we reformulate the reaction rate as follows

$$r_w(u,w) = \begin{cases} \lambda[r(u) - 1] & \text{if } r(u) - 1 \geq 0 \\ -\lambda[r(u) - 1] & \text{if } r(u) - 1 < 0 \text{ and } w > 0 \\ 0 & \text{if } r(u) - 1 < 0 \text{ and } w \leq 0 \end{cases}. \tag{3}$$

The first condition models the case of a positive net precipitation rate, i.e. ions precipitate and form the salt w. The second condition requires that the precipitate w is present, i.e. $w > 0$, and allows for its dissolution. The last equation stops the reaction when the dissolution should occur but the precipitate is not present.

The chemical model we are considering is rather general and it does not depend on the fact that the solutes are transported in a porous media. However, the case of reactive transport in a porous medium has the unique feature that the porous medium itself is influenced by the fact that these reactions, occurring in each spatial point of the domain of interest, can alter its porosity and permeability.

We assume that the solid matrix is formed by two distinct parts: the precipitate w and the solid inert part that does not react. The latter will be called solid rock. In the absence of precipitate the porous media has a prescribed or reference values of porosity and permeability due to the solid rock, named $\overline{\phi}$ and $\overline{k}$ respectively. During the flow of chemical species in the porous media, transported by the liquid phase, a reaction may happen and the deposition of new material is assumed to be around the grains of solid rock or on a layer of precipitate already deposited. See [29] for a more detailed discussion. A graphical representation is given in Figure 1, where we can notice that the deposition of new material alters the flow path in the porous media itself. We can model the change of porosity of porous media by a law which accounts for the dependence on the precipitate concentration as follows

$$\begin{aligned} &\partial_t \phi = -\nu(\phi)\partial_t w \quad t > 0 \\ &\phi(t = 0) = \overline{\phi} \end{aligned} \tag{4}$$

where the precipitate dependent function, which represents the rate of deposition of the solute around the solid rock grains, has the properties

$$\nu \geq 0 \quad \text{and} \quad \phi = 0 \quad \Rightarrow \quad \nu = 0.$$

We notice that when $\phi = 0$ the porous media is occluded and no deposition of new material can take place. Moreover, (4) allows the porosity to increase in presence

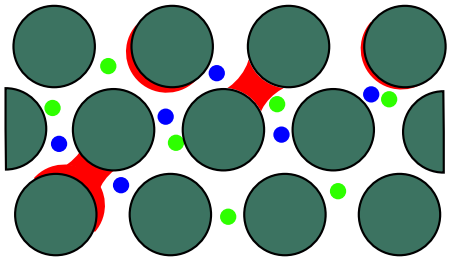

Fig. 1 Graphical representation of a porous media in presence of reactive species. The floating green and blue circles represent the anions and cations flowing in the void space between solid rock grains. The red parts are the deposited material due to the reaction.

of the dissolution of precipitate, conversely the porosity decreases when the precipitate is deposited. Other model can be taken into consideration, but to keep the presentation simpler we adopt (4) where $\nu(\phi) = \eta\phi$, with η a positive constant.

Finally, also the permeability of the porous media is influenced by the reaction. In this work, we consider a Kozeny relationship between the porosity and the permeability k, namely

$$k(\phi) = \bar{k}\frac{\phi^{\alpha}}{\bar{\phi}^{\alpha}}, \tag{5}$$

with $\alpha > 0$ a rock dependent parameter. In this work we chose $\alpha = 2$. More sophisticated models can be found in, e.g., [21].

2.2 Transport model

We introduce now the transport model, assuming that the anions and cations are transported in the porous media as passive scalars. Meaning that there is not a direct influence of the scalar variable u on the given advective field $\boldsymbol{q}$. In addition, we consider a Fick's law to describe the molecular diffusivity of u in the liquid with a coefficient (or tensor) d. The model we are considering for the solute u is given, in its mixed formulation, by

$$\begin{aligned}
&\boldsymbol{\chi} - \boldsymbol{q}u + \phi d\nabla u = \mathbf{0} && \\
&\partial_t(\phi u) + \nabla\cdot\boldsymbol{\chi} + \phi r_w(u,w) = 0 && \text{in } \Omega\times\{t>0\}\\
&\mathrm{tr}\, u = \hat{u} && \text{on } \Gamma_{in}\times\{t>0\}\\
&\mathrm{tr}\,\phi d\nabla u\cdot\boldsymbol{n} = 0 && \text{on } \Gamma_{out}\times\{t>0\}\\
&\mathrm{tr}\,\boldsymbol{\chi}\cdot\boldsymbol{n} = 0 && \text{on } \Gamma_{N}\times\{t>0\}\\
&u(t=0) = \bar{u} && \text{in } \Omega
\end{aligned} \tag{6}$$

With $\boldsymbol{\chi}$ we have denoted the total flux given by the contributions of advection and diffusion. The boundary $\partial\Omega$ of the porous media is divided into three disjoint parts Γ_{in}, Γ_{out}, and Γ_N such that $\overline{\Gamma_{in}} \cup \overline{\Gamma_{out}} \cup \overline{\Gamma_N} = \overline{\partial\Omega}$. The portion Γ_{in} represents the inflow boundary, with $\mathrm{tr}\,\boldsymbol{q} \cdot \boldsymbol{n} < 0$, where the value of u is prescribed as $\hat{u}$. The part Γ_{out} is where the outflow takes place with $\mathrm{tr}\,\boldsymbol{q} \cdot \boldsymbol{n} > 0$. On Γ_N we prescribe zero flux exchange with the outside, we are here assuming that $\mathrm{tr}\,\boldsymbol{q} \cdot \boldsymbol{n} = 0$ in agreement with the boundary conditions of the Darcy problem, see Section 2.3. Other type of boundary conditions can be considered. The outward unit normal of $\partial\Omega$ is indicated with $\boldsymbol{n}$, and the operator tr indicates, in a formal way, a spacial trace operator mapping the variable at the corresponding portion of the boundary $\partial\Omega$. Finally, $\overline{u}$ represents the initial data for the solute.

Problem (6) is an advection-diffusion-reaction equation, which can degenerate due to clogging, i.e. $\phi = 0$ from (4), in some parts of the domain. The reaction term, described by the law (3), is a non-linear and non-smooth function of the solution u and of the precipitate w.

The evolution of the precipitate w follows a similar model of u, with the additional assumption that w does not move in space. All the spatial differential operators are thus removed and we obtain that the model is an ordinary differential equation in each point of Ω, namely

$$\begin{aligned} &\partial_t(\phi w) - \phi r_w(u,w) = 0 && \text{in } \Omega \times \{t > 0\} \\ &w(t=0) = \overline{w} && \text{in } \Omega \end{aligned} \quad . \tag{7}$$

The value $\overline{w}$ represents the initial condition of w in Ω. The reaction terms in the two equations (6) and (7) match each other.

2.3 Darcy model

In this part we introduce the Darcy model and its relation with the previously discussed chemical model. We are interested in computing the Darcy velocity $\boldsymbol{q}$ and the pressure field p in the porous media satisfying the following relations

$$\begin{aligned} &\boldsymbol{q} = -k(\phi)\nabla p \\ &\partial_t \phi + \nabla \cdot \boldsymbol{q} = f && \text{in } \Omega \times \{t > 0\} \\ &\mathrm{tr}\, p = \overline{p} && \Gamma_{in} \times \{t > 0\} \\ &\mathrm{tr}\,\boldsymbol{q} \cdot \boldsymbol{n} = \overline{q} && \Gamma_{out} \times \{t > 0\} \\ &\mathrm{tr}\,\boldsymbol{q} \cdot \boldsymbol{n} = 0 && \Gamma_N \times \{t > 0\} \end{aligned} \quad . \tag{8}$$

The division of the boundary $\partial\Omega$ into parts follows the description given in (6). The boundary value $\overline{p}$ represents the data at the inflow. The value $\overline{q}$ is the outflow flux out of Γ_{out} with the request that $\overline{q} > 0$. The condition on Γ_N is a no flow condition for that portion of boundary. By conservation we obtain that $\mathrm{tr}\,\boldsymbol{q} \cdot \boldsymbol{n} < 0$ on Γ_{in}. Also

in this case other type of boundary conditions can be considered, but they should be coherent with the one prescribed in the model (6).

Equation (8) is coupled with the reactive models (6) and (7) via the dependency of porosity and permeability on the solute u and precipitate w.

2.4 The complete model

The complete model is a six unknowns model and describes the evolution in time and space of: *i)* u solute, *ii)* w precipitate, *iii)* ϕ porosity, *iv)* k permeability, *v)* $\boldsymbol{q}$ Darcy velocity, and *vi)* p pressure. The equations involved are (6), (7), (4), (5), and (8) respectively for each variable or pair of variables. The resulting system is fully coupled, non-smooth and non-linear with possible degeneracy due to vanishing porosity and permeability.

3 A reduced model a fracture

A fracture is a thin object immersed in a porous media, whose aperture is orders of magnitude smaller than any other characteristic size of the problem at hand. The fact that the fracture may exhibit higher or lower permeability with respect to the surrounding porous media increases the problem complexity and requires a proper treatment to obtain an effective and reliable model. The choice adopted here is a reduced model, meaning that the fracture is reduced as an object of lower dimension and new equations and coupling conditions are derived.

In this part, we start by presenting the interface conditions used to couple the porous media and the fracture, being the latter represented as an equi-dimensional object. Then, we present the model reduction procedure to introduce the new model and interface conditions.

3.1 Coupling condition for the equi-dimensional model

Given a parameter $\varepsilon(t)$, called the fracture aperture, which might change in time due to deposition of dissolution of new material. Following the presentation given in [16] we can define the fracture as the domain $\Omega_\gamma(t)$ given by

$$\Omega_\gamma(t) = \left\{ \boldsymbol{x} \in \mathbb{R}^n : \boldsymbol{x} = \boldsymbol{s} + \xi(t)\boldsymbol{n}, \text{ with } \boldsymbol{s} \in \gamma \text{ and } \xi \in \left(-\frac{\varepsilon(\boldsymbol{s},t)}{2}, \frac{\varepsilon(\boldsymbol{s},t)}{2} \right) \right\}, \quad (9)$$

where γ is a non self-intersecting one-codimensional manifold of class C^2. We have $\varepsilon(\cdot,t) \in C^2(\gamma)$ and we assume that the fracture aperture varies slowly compare to the

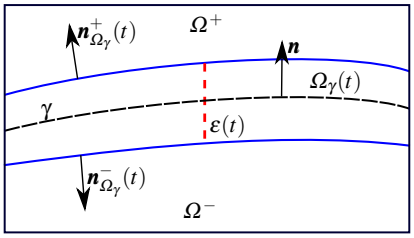

Fig. 2 Equi-dimensional representation of a fracture Ω_γ immersed in a porous media Ω.

local coordinate system. The vector $\boldsymbol{n}$ is the normal vector of γ pointing towards one of the side of the surrounding porous media. This choice of orientation is arbitrary and will not change the following procedure. Finally, to ease the presentation we suppose that the fracture cuts the porous media in two disjoint parts indicated with $+$ and $-$. Extension to more general cases are straightforward. An example is reported in Figure 2.

Being Ω_γ equi-dimensional with respect to the surrounding porous media Ω it is possible to write the same equations to model the reactive transport as the one discussed in Subsection 2.4 but applied to Ω_γ instead. We will indicate with a subscript if the variable or data is referred to the porous media Ω or to the equi-dimensional representation of the fracture Ω_γ.

In addition to this, interface conditions have to be considered to couple the two problems at their common boundaries. For the transport equation (6), following [19], we have the conservation of the total flux and the continuity of the solute u, meaning

$$\begin{aligned} \operatorname{tr} \boldsymbol{\chi}_\Omega \cdot \boldsymbol{n}_{\Omega_\gamma} &= \operatorname{tr} \boldsymbol{\chi}_{\Omega_\gamma} \cdot \boldsymbol{n}_{\Omega_\gamma} \\ \operatorname{tr} u_\Omega &= \operatorname{tr} u_{\Omega_\gamma} \end{aligned} \qquad \text{on } \partial\Omega \cap \partial\Omega_\gamma, \tag{10}$$

where $\boldsymbol{n}_{\Omega_\gamma}$ is the unit normal of the boundary of Ω_γ pointing from the latter toward Ω. For the Darcy equation (8) across the interfaces we have continuity of the normal component of Darcy velocity $\boldsymbol{q}$ as well as the continuity of the pressure p. Following [27, 15, 32] we obtain

$$\begin{aligned} \operatorname{tr} \boldsymbol{q}_\Omega \cdot \boldsymbol{n}_{\Omega_\gamma} &= \operatorname{tr} \boldsymbol{q}_{\Omega_\gamma} \cdot \boldsymbol{n}_{\Omega_\gamma} \\ \operatorname{tr} p_\Omega &= \operatorname{tr} p_{\Omega_\gamma} \end{aligned} \qquad \text{on } \partial\Omega \cap \partial\Omega_\gamma. \tag{11}$$

Finally, the full equi-dimensional model for porous media-fracture system is given by equations (6), (7), (4), (5), and (8) for both Ω and Ω_γ along with the coupling conditions given by (10) and (11).

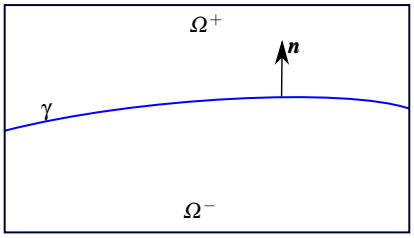

Fig. 3 Hybrid-dimensional representation of a fracture immersed in a porous media.

3.2 The reduced variables

The model reduction procedure approximates the equi-dimensional representation of the fracture Ω_γ by its centre line γ, and derive new equations to describe the variables in γ and new interface conditions for the coupling with the surrounding porous media. Due to the previously mentioned assumptions on γ, we approximate $\boldsymbol{n}^{\pm}_{\Omega_\gamma}$ with $\pm\boldsymbol{n}$. The representation of $\Omega \subset \mathbb{R}^n$ and γ as co-dimension one object is usually named as hybrid-dimensional. See Figure 3 as an example.

The new variables defined on γ are defined differently if they are scalar or vector fields. In the former case we define average values as

$$u_\gamma(\boldsymbol{s},t) = \frac{1}{\varepsilon(\boldsymbol{s},t)} \int_{-\frac{\varepsilon(\boldsymbol{s},t)}{2}}^{\frac{\varepsilon(\boldsymbol{s},t)}{2}} u_{\Omega_\gamma}(t) d\boldsymbol{n}(\boldsymbol{s}) \quad \text{and} \quad p_\gamma(\boldsymbol{s}) = \frac{1}{\varepsilon(\boldsymbol{s},t)} \int_{-\frac{\varepsilon(\boldsymbol{s},t)}{2}}^{\frac{\varepsilon(\boldsymbol{s},t)}{2}} p_{\Omega_\gamma}(t) d\boldsymbol{n}(\boldsymbol{s}), \tag{12}$$

where $\boldsymbol{s} \in \gamma$ and the time dependent integrals are done along the direction normal to the fracture γ. For the vector fields $\boldsymbol{\chi}$ and $\boldsymbol{q}$ we need to introduce the following projection matrices along and across the fracture, given by

$$N = \boldsymbol{n} \otimes \boldsymbol{n} \quad \text{and} \quad T = I - N.$$

Now, we can define

$$\boldsymbol{\chi}_\gamma = \int_{-\frac{\varepsilon(\boldsymbol{s},t)}{2}}^{\frac{\varepsilon(\boldsymbol{s},t)}{2}} T(\boldsymbol{s}) \boldsymbol{\chi}_{\Omega_\gamma}(t) d\boldsymbol{n}(\boldsymbol{s}) \quad \text{and} \quad \boldsymbol{q}_\gamma = \int_{-\frac{\varepsilon(\boldsymbol{s},t)}{2}}^{\frac{\varepsilon(\boldsymbol{s},t)}{2}} T(\boldsymbol{s}) \boldsymbol{q}_{\Omega_\gamma}(t) d\boldsymbol{n}(\boldsymbol{s}) \tag{13}$$

which, it is worth to notice, are not average values of fluxes or velocity, but time dependent integrals. We require that, following the idea of [2, 27], the permeability for the fracture (8) is aligned to the local coordinate system, meaning that we have

$$k_{\Omega_\gamma} = k_\gamma T + \kappa N, \tag{14}$$

where k_γ is a square tensor of dimension $n-1$, symmetric and positive defined, and κ is a positive real number. Moreover, also the diffusion tensor of equation (6) is required to follow the similar request

$$d_{\Omega_\gamma} = d_\gamma T + \delta N,$$

where d_γ is a square tensor of dimension $n-1$, symmetric and positive defined, and δ is a positive real number.

Finally, the fracture is initially considered open, meaning $\phi_{\Omega_\gamma} = 1$, and in the reduced model its role will be played by the aperture ε. We will give a specific law for its evolution. This will be part of the discussion in Subsection 3.4.

3.3 Reduced transport model

We describe now the procedure to derive the reduced model for the system (6). First of all the first equation of (6) is decomposed in its normal and tangential parts as

$$\begin{aligned} T\boldsymbol{\chi}_{\Omega_\gamma} - T\boldsymbol{q}_{\Omega_\gamma} u_{\Omega_\gamma} + T d_{\Omega_\gamma} \nabla u_{\Omega_\gamma} &= \mathbf{0}, \\ N\boldsymbol{\chi}_{\Omega_\gamma} - N\boldsymbol{q}_{\Omega_\gamma} u_{\Omega_\gamma} + N d_{\Omega_\gamma} \nabla u_{\Omega_\gamma} &= \mathbf{0}. \end{aligned} \tag{15}$$

Now, the tangential equation is integrated in the normal direction $\boldsymbol{n}$ across the fracture. Dropping the dependency on $\boldsymbol{s}$ and t when not needed, we obtain

$$\int_{-\frac{\varepsilon}{2}}^{\frac{\varepsilon}{2}} T\boldsymbol{\chi}_{\Omega_\gamma} d\boldsymbol{n} - \int_{-\frac{\varepsilon}{2}}^{\frac{\varepsilon}{2}} T\boldsymbol{q}_{\Omega_\gamma} u_{\Omega_\gamma} d\boldsymbol{n} + \int_{-\frac{\varepsilon}{2}}^{\frac{\varepsilon}{2}} T d_{\Omega_\gamma} \nabla u_{\Omega_\gamma} d\boldsymbol{n} = \mathbf{0},$$

having $T d_{\Omega_\gamma} = T d_\gamma$ and by assuming small variations of along the thickness of the fracture of $\boldsymbol{q}_\gamma$ and u_γ, we get the following expression

$$\boldsymbol{\chi}_\gamma - \boldsymbol{q}_\gamma u_\gamma + \varepsilon d_\gamma \nabla_T u_\gamma = \mathbf{0} \qquad \text{in } \gamma \times \{t > 0\}, \tag{16}$$

where the nabla operator $\nabla_T = T\nabla$ is defined now on the tangent space of the fracture. The second equation of (15) gives the coupling conditions between the fracture γ and the surrounding porous medium, i.e. the sides Ω^+ and Ω^-. The derivation of such conditions requires the integration from the centre line of Ω_γ to its boundary, which is given, for Ω^+, by

$$\int_0^{\frac{\varepsilon}{2}} N\boldsymbol{\chi}_{\Omega_\gamma} \cdot \boldsymbol{n} d\boldsymbol{n} - \int_0^{\frac{\varepsilon}{2}} N\boldsymbol{q}_{\Omega_\gamma} u_{\Omega_\gamma} \cdot \boldsymbol{n} d\boldsymbol{n} + \int_0^{\frac{\varepsilon}{2}} N d_{\Omega_\gamma} \nabla u_{\Omega_\gamma} \cdot \boldsymbol{n} d\boldsymbol{n} = 0.$$

For the last term, we have $N d_{\Omega_\gamma} = N\delta$ and it can be approximated as

$$\int_0^{\frac{\varepsilon}{2}} N\delta \nabla u_{\Omega_\gamma} \cdot \boldsymbol{n} d\boldsymbol{n} \approx \delta(\operatorname{tr} u_{\Omega^+} - u_\gamma).$$

While for the other two terms we consider a first order one-side integration rule, along with the continuity conditions (10) and (11) for its approximation. We get

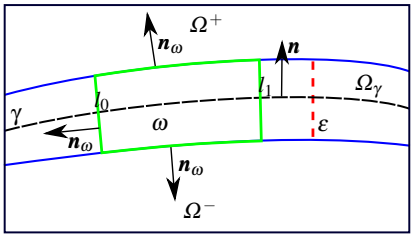

Fig. 4 Equi-dimensional representation of a fracture immersed in a porous media with the control volume ω.

$$\int_0^{\frac{\varepsilon}{2}} N\boldsymbol{\chi}_{\Omega_\gamma}\cdot\boldsymbol{n}d\boldsymbol{n}-\int_0^{\frac{\varepsilon}{2}} N\boldsymbol{q}_{\Omega_\gamma}u_{\Omega_\gamma}\cdot\boldsymbol{n}d\boldsymbol{n}\approx\frac{\varepsilon}{2}\left(\operatorname{tr}\boldsymbol{\chi}_{\Omega^+}\cdot\boldsymbol{n}-\operatorname{tr}\boldsymbol{q}_{\Omega^+}\cdot\boldsymbol{n}\operatorname{tr}u_{\Omega^+}\right).$$

Finally, we get the coupling condition for the side of the fracture in contact with Ω^+

$$\varepsilon\left(\operatorname{tr}\boldsymbol{\chi}_{\Omega^+}\cdot\boldsymbol{n}-\operatorname{tr}\boldsymbol{q}_{\Omega^+}\cdot\boldsymbol{n}\operatorname{tr}u_{\Omega^+}\right)=2\delta(u_\gamma-\operatorname{tr}u_{\Omega^+}) \tag{17}$$

For the other side Ω^- the derivation is similar.

The conservation equation, second of (6), is reduced following the same approach presented in [7]. Its integral form is given by

$$\partial_t\int_{\omega(t)}u_{\Omega_\gamma}d\boldsymbol{x}+\int_{\partial\omega(t)}\operatorname{tr}\boldsymbol{\chi}_{\Omega_\gamma}\cdot\boldsymbol{n}_\omega d\boldsymbol{\sigma}+\int_{\omega(t)}r_w(u_{\Omega_\gamma},w_{\Omega_\gamma})d\boldsymbol{x}=0 \tag{18}$$

where $\omega(t)=(l_0,l_1)\times(-\varepsilon(t)/2,\varepsilon(t)/2)\subset\Omega_\gamma(t)$ and with $(l_0,l_1)\subset\gamma$. Note that the latter does not depend on time. The vector $\boldsymbol{n}_\omega$ is the outward unit normal of ω. See Figure 4 for a more detailed representation of the objects involved. The first and third part of the previous equation, omitting the dependency on t, are now given by

$$\int_{l_0}^{l_1}\left(\partial_t\int_{-\frac{\varepsilon}{2}}^{\frac{\varepsilon}{2}}u_{\Omega_\gamma}d\boldsymbol{n}+\int_{-\frac{\varepsilon}{2}}^{\frac{\varepsilon}{2}}r_w(u_{\Omega_\gamma},w_{\Omega_\gamma})d\boldsymbol{n}\right)d\boldsymbol{s}=\int_{l_0}^{l_1}\partial_t(\varepsilon u_\gamma)+\varepsilon r_w(u_\gamma,w_\gamma)d\boldsymbol{s}$$

The second part of (18) becomes

$$\int_{\partial\omega}\operatorname{tr}\boldsymbol{\chi}_{\Omega_\gamma}\cdot\boldsymbol{n}_\omega d\boldsymbol{\sigma}=\int_{\partial\Omega_\gamma\cap\partial\omega}\operatorname{tr}\boldsymbol{\chi}_{\Omega_\gamma}\cdot\boldsymbol{n}_{\Omega_\gamma}d\boldsymbol{\sigma}+\int_{\partial\omega^+}\operatorname{tr}\boldsymbol{\chi}_{\Omega_\gamma}\cdot\boldsymbol{n}_\omega d\boldsymbol{\sigma}+\int_{\partial\omega^-}\operatorname{tr}\boldsymbol{\chi}_{\Omega_\gamma}\cdot\boldsymbol{n}_\omega d\boldsymbol{\sigma},$$

with $\partial\omega^+=\{l_1\}\times(-\varepsilon/2,\varepsilon/2)$ and $\partial\omega^-=\{l_0\}\times(-\varepsilon/2,\varepsilon/2)$. Now, setting $|(l_0,l_1)|\to 0$ we obtain the following expressions

$$\lim_{|(l_0,l_1)|\to 0} \frac{1}{|(l_0,l_1)|} \int_{l_0}^{l_1} \partial_t(\varepsilon u_\gamma) + \varepsilon r_w(u_\gamma, w_\gamma) d\boldsymbol{s} = \partial_t(\varepsilon u_\gamma) + \varepsilon r_w(u_\gamma, w_\gamma)$$
$$\lim_{|(l_0,l_1)|\to 0} \frac{1}{|(l_0,l_1)|} \int_{\partial\omega} \operatorname{tr} \boldsymbol{\chi}_{\Omega_\gamma} \cdot \boldsymbol{n}_\omega d\boldsymbol{\sigma} = \operatorname{tr} \boldsymbol{\chi}_{\Omega_\gamma} \cdot \boldsymbol{n}_{\Omega_\gamma}|_{\frac{\varepsilon}{2}} + \operatorname{tr} \boldsymbol{\chi}_{\Omega_\gamma} \cdot \boldsymbol{n}_{\Omega_\gamma}|_{-\frac{\varepsilon}{2}} + \nabla_T \cdot \boldsymbol{\chi}_\gamma$$

by using the continuity conditions (10) the last equation becomes

$$\lim_{|(l_0,l_1)|\to 0} \frac{1}{|(l_0,l_1)|} \int_{\partial\omega} \operatorname{tr} \boldsymbol{\chi}_{\Omega_\gamma} \cdot \boldsymbol{n}_\omega d\boldsymbol{\sigma} = \operatorname{tr} \boldsymbol{\chi}_{\Omega^+} \cdot \boldsymbol{n} - \operatorname{tr} \boldsymbol{\chi}_{\Omega^-} \cdot \boldsymbol{n} + \nabla_T \cdot \boldsymbol{\chi}_\gamma.$$

Finally, the conservation equation for the transport system of the solute is reduced as

$$\begin{aligned} &\partial_t(\varepsilon u_\gamma) + \nabla_T \cdot \boldsymbol{\chi}_\gamma + \operatorname{tr} \boldsymbol{\chi}_{\Omega^+} \cdot \boldsymbol{n} - \operatorname{tr} \boldsymbol{\chi}_{\Omega^-} \cdot \boldsymbol{n} + \varepsilon r_w(u_\gamma, w_\gamma) = 0 && \text{in } \gamma \times \{t > 0\} \\ &u_\gamma(t=0) = \overline{u}_\gamma && \text{in } \gamma \end{aligned}, \tag{19}$$

where $\overline{u}_\gamma$ is the reduced initial condition, given by $\overline{u}_\gamma = \frac{1}{\varepsilon} \int_{-\frac{\varepsilon}{2}}^{\frac{\varepsilon}{2}} \overline{u}_{\Omega_\gamma}$. The reduced boundary conditions for the transport problem are given by the following

$$\begin{aligned} &\operatorname{tr} u_\gamma = \hat{u}_\gamma && \text{on } (\partial\gamma \cap \Gamma_{in}) \times \{t > 0\} \\ &\operatorname{tr} \varepsilon d_\gamma \nabla_T u_\gamma \cdot \boldsymbol{n} = 0 && \text{on } (\partial\gamma \cap \Gamma_{out}) \times \{t > 0\}, \\ &\operatorname{tr} \boldsymbol{\chi}_\gamma \cdot \boldsymbol{n} = 0 && \text{on } (\partial\gamma \cap \Gamma_N) \times \{t > 0\} \end{aligned} \tag{20}$$

where $\hat{u}_\gamma$ is defined accordingly. We have assumed here that, for example if γ is one-dimensional, a single boundary condition is assigned to each end point $\partial\gamma$.

For the precipitate the derivation of the reduced model is rather easy since no spatial differential operators are involved. From (7) and by considering again the control volume $\omega(t)$, we get

$$\partial_t \int_{\omega(t)} w_{\Omega_\gamma} d\boldsymbol{x} - \int_{\omega(t)} r_w(u_{\Omega_\gamma}, w_{\Omega_\gamma}) d\boldsymbol{x} = 0$$

and proceeding as before we obtain

$$\lim_{|(l_0,l_1)|\to 0} \frac{1}{|(l_0,l_1)|} \int_{l_0}^{l_1} \left(\partial_t \int_{-\frac{\varepsilon}{2}}^{\frac{\varepsilon}{2}} w_{\Omega_\gamma} d\boldsymbol{n} - \int_{-\frac{\varepsilon}{2}}^{\frac{\varepsilon}{2}} r_w(u_{\Omega_\gamma}, w_{\Omega_\gamma}) d\boldsymbol{n} \right) d\boldsymbol{s} =$$
$$\lim_{|(l_0,l_1)|\to 0} \frac{1}{|(l_0,l_1)|} \int_{l_0}^{l_1} \partial_t(\varepsilon w_\gamma) - \varepsilon r_w(u_\gamma, w_\gamma) d\boldsymbol{s} = \partial_t(\varepsilon w_\gamma) - \varepsilon r_w(u_\gamma, w_\gamma).$$

Finally, the following is the reduced model for the precipitate w

$$\begin{aligned} &\partial_t(\varepsilon w_\gamma) - \varepsilon r_w(u_\gamma, w_\gamma) = 0 && \text{in } \gamma \times \{t > 0\} \\ &w_\gamma(t=0) = \overline{w}_\gamma && \text{in } \gamma \end{aligned}, \tag{21}$$

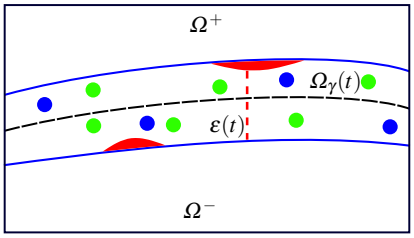

Fig. 5 Equi-dimensional representation of a fracture immersed in a porous media with dynamics of deposition and dissolution due to the chemical reaction. The solutes are the blue and green circles and the precipitate is depicted in red.

where $\overline{w}_\gamma$ is the reduced initial condition for w_γ, given by $\overline{w}_\gamma = \frac{1}{\varepsilon}\int_{-\frac{\varepsilon}{2}}^{\frac{\varepsilon}{2}} \overline{w}_{\Omega_\gamma}$.

3.4 Aperture and permeability models

Following the ideas discussed in [26], to derive the variation of the fracture aperture by the deposition or dissolution of the solute, we consider a law similar to the one given for the porosity in (4). However, in this case since the fracture is supposed to be initially empty, free from granular material, we assume that the new material is accumulated or dissolved at the fracture boundary. See Figure 5 for a graphical representation. We consider again a precipitate dependent law to describe the rate of aperture change, we have

$$\begin{aligned} &\partial_t \varepsilon = -\upsilon(\varepsilon)\partial_t w_\gamma \quad t > 0 \\ &\varepsilon(t=0) = \overline{\varepsilon} \end{aligned} \tag{22}$$

where the aperture dependent model, which represents the rate of deposition of the solute around the fracture walls, has the following properties

$$\upsilon \geq 0 \quad \text{and} \quad \varepsilon = 0 \quad \Rightarrow \quad \upsilon = 0.$$

We notice that when $\varepsilon = 0$ the fracture is occluded and no deposition of new material takes place. Moreover, (22) allows the aperture to increase in presence of the dissolution of precipitate, conversely the aperture decreases when the precipitate is deposited. Other models can be taken into consideration, but to keep the presentation simpler we adopt (22) where $\upsilon(\varepsilon) = \eta_\gamma \varepsilon$, with η_γ a positive constant. In (22), the value of $\overline{\varepsilon} \geq 0$ represents the initial aperture of the fracture.

The fracture permeability, both normal κ and tangential k_γ are now related to the fracture aperture by the cubic law

$$k_\gamma = \overline{k}_\gamma \frac{\varepsilon^2}{\overline{\varepsilon}} \quad \text{and} \quad \kappa = \overline{\kappa}\frac{\varepsilon^2}{\overline{\varepsilon}}. \tag{23}$$

Here $\overline{k}_\gamma$, symmetric and positive defined, and $\overline{\kappa} > 0$ are the reference tangential and normal fracture permeability, respectively.

3.4.1 Reduced Darcy model

In this part we derive the reduced model for the Darcy system (8) written in the fracture. The steps are rather similar to the one presented for the transport equation with few modifications. The Darcy equation, first of (8) is projected on the tangential and normal directions of the fracture obtaining

$$\begin{aligned} T\boldsymbol{q}_{\Omega_\gamma} + Tk_{\Omega_\gamma}\nabla p_{\Omega_\gamma} &= \mathbf{0}, \\ N\boldsymbol{q}_{\Omega_\gamma} + Nk_{\Omega_\gamma}\nabla p_{\Omega_\gamma} &= \mathbf{0}. \end{aligned} \tag{24}$$

The first of (24) is now integrated across the normal section of the fracture, along the direction given by $\boldsymbol{n}$. We have

$$\int_{-\frac{\varepsilon}{2}}^{\frac{\varepsilon}{2}} T\boldsymbol{q}_{\Omega_\gamma} d\boldsymbol{n} + \int_{-\frac{\varepsilon}{2}}^{\frac{\varepsilon}{2}} Tk_{\Omega_\gamma}\nabla p_{\Omega_\gamma} d\boldsymbol{n} = \mathbf{0}.$$

From the assumption on the permeability (14) we obtain $Tk_{\Omega_\gamma} = Tk_\gamma$. By assuming small variations along the thickness of the fracture of ∇p_{Ω_γ}, we get the following relation

$$\boldsymbol{q}_\gamma + \varepsilon k_\gamma \nabla_T p_\gamma = \mathbf{0} \quad \text{in} \quad \gamma \times \{t > 0\}. \tag{25}$$

The second relation in (24) gives the coupling conditions between the fracture and the surrounding porous media for the Darcy problem. The approach is similar to the one already presented for the transport part, we integrate the second of (24) from 0 to $\varepsilon/2$ and we do some approximation of the integrals involved. We start with

$$\int_0^{\frac{\varepsilon}{2}} N\boldsymbol{q}_{\Omega_\gamma} \cdot \boldsymbol{n} + \int_0^{\frac{\varepsilon}{2}} Nk_{\Omega_\gamma}\nabla p_{\Omega_\gamma} \cdot \boldsymbol{n} = \mathbf{0}.$$

The first integral is approximated by a one-side integration rule and the coupling conditions (11) are considered to get

$$\int_0^{\frac{\varepsilon}{2}} N\boldsymbol{q}_{\Omega_\gamma} \cdot \boldsymbol{n} \approx \frac{\varepsilon}{2} \operatorname{tr} \boldsymbol{q}_{\Omega^+} \cdot \boldsymbol{n},$$

while recognising that $Nk_{\Omega_\gamma} = N\kappa$, for the second term we obtain

$$\int_0^{\frac{\varepsilon}{2}} Nk_{\Omega_\gamma}\nabla p_{\Omega_\gamma} \cdot \boldsymbol{n} \approx \kappa(\operatorname{tr} p_{\Omega^+} - p_\gamma).$$

The coupling conditions of the reduced model for the Darcy equation, for the side of the fracture in contact with Ω^+, are thus given by

$$\varepsilon \operatorname{tr} \boldsymbol{q}_{\Omega^+} \cdot \boldsymbol{n} = 2\kappa(\operatorname{tr} p_{\Omega^+} - p_\gamma). \tag{26}$$

Also in this case, for the side Ω^- the derivation of the coupling conditions are similar.

Finally, to complete the Darcy system the conservation equation for the fracture has to be reduced. Unlike the previous steps, which are in agreement with the existing literature, see for instance [27, 16, 7], this last step differ from the previous works on model reduction for fractured media because we have to account for a time dependent aperture. We consider again the control volume $\omega(t)$ given as before, and the integral form of the conservation equation is given by

$$\partial_t \int_{\omega(t)} d\boldsymbol{x} + \int_{\partial\omega(t)} \operatorname{tr} \boldsymbol{q}_{\Omega_\gamma} \cdot \boldsymbol{n}_\omega d\boldsymbol{\sigma} = \int_{\omega(t)} f d\boldsymbol{x}. \tag{27}$$

Reminding that $\omega(t) = (l_0, l_1) \times (-\varepsilon(t)/2, \varepsilon(t)/2)$, the first and last terms, dropping the dependence on t, can be expressed as

$$\lim_{|(l_0,l_1)|\to 0} \frac{1}{|(l_0,l_1)|} \int_{l_0}^{l_1} \left(\partial_t \int_{-\frac{\varepsilon}{2}}^{\frac{\varepsilon}{2}} d\boldsymbol{n} - \int_{-\frac{\varepsilon}{2}}^{\frac{\varepsilon}{2}} f d\boldsymbol{n} \right) d\boldsymbol{s} = \partial_t \varepsilon - \varepsilon f_\gamma,$$

where f_γ is the reduced source or sink term expressed by $f_\gamma = \frac{1}{\varepsilon} \int_{-\frac{\varepsilon}{2}}^{\frac{\varepsilon}{2}} f d\boldsymbol{n}$. The second term in (27) becomes

$$\int_{\partial\omega} \operatorname{tr} \boldsymbol{q}_{\Omega_\gamma} \cdot \boldsymbol{n}_\omega d\boldsymbol{\sigma} = \int_{\partial\Omega_\gamma \cap \partial\omega} \operatorname{tr} \boldsymbol{q}_{\Omega_\gamma} \cdot \boldsymbol{n}_\omega d\boldsymbol{\sigma} + \int_{\partial\omega^+} \operatorname{tr} \boldsymbol{q}_{\Omega_\gamma} \cdot \boldsymbol{n}_\omega d\boldsymbol{\sigma} + \int_{\partial\omega^-} \operatorname{tr} \boldsymbol{q}_{\Omega_\gamma} \cdot \boldsymbol{n}_\omega d\boldsymbol{\sigma}.$$

By shrinking the domain ω as $|(l_0, l_1)| \to 0$ the last relation becomes

$$\lim_{|(l_0,l_1)|\to 0} \frac{1}{|(l_0,l_1)|} \int_{\partial\omega} \operatorname{tr} \boldsymbol{q}_{\Omega_\gamma} \cdot \boldsymbol{n}_\omega d\boldsymbol{\sigma} = \operatorname{tr} \boldsymbol{q}_{\Omega_\gamma} \cdot \boldsymbol{n}_\omega|_{\frac{\varepsilon}{2}} + \operatorname{tr} \boldsymbol{q}_{\Omega_\gamma} \cdot \boldsymbol{n}_\omega|_{-\frac{\varepsilon}{2}} + \nabla_T \cdot \boldsymbol{q}_\gamma,$$

and by using the continuity condition at the fracture-porous media boundary (11) we finally get

$$\lim_{|(l_0,l_1)|\to 0} \frac{1}{|(l_0,l_1)|} \int_{\partial\omega} \operatorname{tr} \boldsymbol{q}_{\Omega_\gamma} \cdot \boldsymbol{n}_\omega d\boldsymbol{\sigma} = \operatorname{tr} \boldsymbol{q}_{\Omega^+} \cdot \boldsymbol{n} - \operatorname{tr} \boldsymbol{q}_{\Omega^-} \cdot \boldsymbol{n} + \nabla_T \cdot \boldsymbol{q}_\gamma.$$

To conclude the conservation equation for the Darcy flow is given by

$$\partial_t \varepsilon + \nabla_T \cdot \boldsymbol{q}_\gamma + \operatorname{tr} \boldsymbol{q}_{\Omega^+} \cdot \boldsymbol{n} - \operatorname{tr} \boldsymbol{q}_{\Omega^-} \cdot \boldsymbol{n} = \varepsilon f_\gamma \quad \text{in } \gamma \times \{t > 0\}. \tag{28}$$

The reduced boundary conditions for the Darcy problem are given by the following

$$\begin{aligned} \operatorname{tr} p_\gamma &= \overline{p}_\gamma \qquad (\partial\gamma \cap \Gamma_{in}) \times \{t > 0\} \\ \operatorname{tr} \boldsymbol{q}_\gamma \cdot \boldsymbol{n} &= \overline{q}_\gamma \quad (\partial\gamma \cap \Gamma_{out}) \times \{t > 0\}, \\ \operatorname{tr} \boldsymbol{q}_\gamma \cdot \boldsymbol{n} &= 0 \qquad (\partial\gamma \cap \Gamma_N) \times \{t > 0\} \end{aligned} \tag{29}$$

with $\overline{p}_\gamma$ and $\overline{q}_\gamma$ being defined accordingly.

3.4.2 The complete reduced model

We can now summarize the full hybrid-dimensional problem, in this case we have six fields for the porous media and seven other fields for the fractures. For the former the reader can refer to the description given in Subsection 2.4 for Ω, which in the latter we have the evolution of: *i)* u_γ solute, *ii)* w_γ precipitate, *iii)* ε aperture, *iv)* κ and k_γ normal and tangential permeability, *v)* $\boldsymbol{q}_\gamma$ Darcy velocity, and *vi)* p_γ pressure.

For the fracture the equations involved are (16), (17), (2.4), and (20) for u_γ. For w_γ the problem (21), and for ε (22). For the permeabilities κ and k_γ the model given by (23). Finally, for $\boldsymbol{q}_\gamma$ and p_γ the equations (25), (26), (28), and (29).

Finally, it is important to mention that due to the model reduction procedure the aperture is now a time dependent model parameter and not any more a geometrical constraint for the problem.

4 Conclusion

In this work we have presented a reduced model for fluid flow in fractured porous media. The liquid phase flow is governed by the Darcy law and, dissolved in the liquid itself, chemical species (solutes) can react and precipitate forming a salt (or an immobile phase that fills the void spaces). Moreover, the latter can also dissolve to form solutes. The dissolution or precipitation processes can alter the porosity of the porous media, changing thus the Darcy velocity of the liquid. As mentioned, we have assumed that in the porous medium a fracture is present which may dramatically alter the flow properties of the system and thus requires an adequate model to obtain reliable and accurate results. What we have proposed is a reduced model that leads to a hybrid-dimensional framework, where the fracture is one dimensional smaller than the porous medium itself. New equations have been derived to model the physical processes in the fracture as well as the coupling conditions between the fracture itself and the surrounding porous media. The complete set of equations forms a reactive transport model in a fractured porous medium. An extension, which will be part of a future work, is the introduction of a discrete setting for the efficient solution of the proposed mathematical model.

References

1. Agosti, A., Formaggia, L., Scotti, A.: Analysis of a model for precipitation and dissolution coupled with a darcy flux. Journal of Mathematical Analysis and Applications **431**(2), 752–781 (2015). DOI https://doi.org/10.1016/j.jmaa.2015.06.003. URL http://www.sciencedirect.com/science/article/pii/S0022247X15005466
2. Alboin, C., Jaffré, J., Roberts, J.E., Serres, C.: Modeling fractures as interfaces for flow and transport in porous media. In: Fluid flow and transport in porous media: mathematical and numerical treatment (South Hadley, MA, 2001), Contemp. Math., vol. 295, pp. 13–24. Amer. Math. Soc., Providence, RI (2002)
3. Ambartsumyan, I., Khattatov, E., Nguyen, T., Yotov, I.: Flow and transport in fractured poroelastic media. GEM - International Journal on Geomathematics **10**(1), 11 (2019). DOI 10.1007/s13137-019-0119-5. URL https://doi.org/10.1007/s13137-019-0119-5
4. Antonietti, P.F., Formaggia, L., Scotti, A., Verani, M., Verzotti, N.: Mimetic finite difference approximation of flows in fractured porous media. ESAIM: M2AN **50**(3), 809–832 (2016). DOI 10.1051/m2an/2015087. URL http://dx.doi.org/10.1051/m2an/2015087
5. Berge, R., Berre, I., Keilegavlen, E., Wohlmuth, B.: Finite volume discretization for poroelastic media with fractures modeled by contact mechanics. Tech. rep., arXiv:1904.11916 [math.NA] (2019). URL https://arxiv.org/abs/1904.11916
6. Berre, I., Doster, F., Keilegavlen, E.: Flow in fractured porous media: A review of conceptual models and discretization approaches. Transport in Porous Media **130**(1), 215–236 (2019). DOI 10.1007/s11242-018-1171-6. URL https://doi.org/10.1007/s11242-018-1171-6
7. Boon, W.M., Nordbotten, J.M., Yotov, I.: Robust discretization of flow in fractured porous media. SIAM Journal on Numerical Analysis **56**(4), 2203–2233 (2018). DOI 10.1137/17M1139102. URL https://doi.org/10.1137/17M1139102
8. Bukac, M., Yotov, I., Zunino, P.: Dimensional model reduction for flow through fractures in poroelastic media. ESAIM: Mathematical Modelling and Numerical Analysis **51**(4), 1429–1471 (2017). DOI 10.1051/m2an/2016069. URL https://doi.org/10.1051/m2an/2016069
9. Chave, F., Di Pietro, D.A., Formaggia, L.: A hybrid high-order method for darcy flows in fractured porous media. SIAM Journal on Scientific Computing **40**(2), A1063–A1094 (2018). DOI 10.1137/17M1119500. URL https://doi.org/10.1137/17M1119500
10. Chave, F., Di Pietro, D.A., Formaggia, L.: A hybrid high-order method for passive transport in fractured porous media. GEM - International Journal on Geomathematics **10**(1), 12 (2019). DOI 10.1007/s13137-019-0114-x. URL https://doi.org/10.1007/s13137-019-0114-x
11. D'Angelo, C., Scotti, A.: A mixed finite element method for Darcy flow in fractured porous media with non-matching grids. Mathematical Modelling and Numerical Analysis **46**(02), 465–489 (2012). DOI 10.1051/m2an/2011148
12. van Duijn, C., Pop, I.S.: Crystal dissolution and precipitation in porous media : pore scale analysis. Journal für die reine und angewandte Mathematik (Crelle's Journal) **577**, 171–211 (2004). DOI 10.1515/crll.2004.2004.577.171
13. Elyes, A., Jérôme, J., Roberts, J.E.: A 3-D reduced fracture model for two-phase flow in porous media with a global pressure formulation. In: MAMERN VI. Pau, France (2015). URL https://hal.inria.fr/hal-01119986
14. Emmanuel, S., Berkowitz, B.: Mixing-induced precipitation and porosity evolution in porous media. Advances in Water Resources **28**(4), 337–344 (2005). DOI https://doi.org/10.1016/j.advwatres.2004.11.010. URL http://www.sciencedirect.com/science/article/pii/S030917080400212X
15. Faille, I., Fumagalli, A., Jaffré, J., Roberts, J.E.: Model reduction and discretization using hybrid finite volumes of flow in porous media containing faults. Computational Geosciences **20**(2), 317–339 (2016). DOI 10.1007/s10596-016-9558-3. URL https://link.springer.com/article/10.1007/s10596-016-9558-3
16. Formaggia, L., Fumagalli, A., Scotti, A., Ruffo, P.: A reduced model for Darcy's problem in networks of fractures. ESAIM: Mathematical Modelling and Numerical Analysis **48**, 1089–1116 (2014). DOI 10.1051/m2an/2013132. URL https://www.esaim-m2an.org/articles/m2an/abs/2014/04/m2an130132/m2an130132.html

17. Fumagalli, A., Keilegavlen, E.: Dual virtual element methods for discrete fracture matrix models. Oil & Gas Science and Technology - Revue d'IFP Energies nouvelles **74**(41), 1–17 (2019). DOI doi.org/10.2516/ogst/2019008
18. Fumagalli, A., Scotti, A.: A numerical method for two-phase flow in fractured porous media with non-matching grids. Advances in Water Resources **62, Part C**(0), 454–464 (2013). DOI 10.1016/j.advwatres.2013.04.001. URL https://www.sciencedirect.com/science/article/pii/S0309170813000523. Computational Methods in Geologic CO2 Sequestration
19. Fumagalli, A., Scotti, A.: A Reduced Model for Flow and Transport in Fractured Porous Media with Non-matching Grids. In: A. Cangiani, R.L. Davidchack, E. Georgoulis, A.N. Gorban, J. Levesley, M.V. Tretyakov (eds.) Numerical Mathematics and Advanced Applications 2011, pp. 499–507. Springer Berlin Heidelberg (2013). DOI 10.1007/978-3-642-33134-3_53
20. Ganis, B., Girault, V., Mear, M., Singh, G., Wheeler, M.: Modeling fractures in a poro-elastic medium. Oil & Gas Science and Technology–Revue d'IFP Energies nouvelles **69**(4), 515–528 (2014)
21. Hommel, J., Coltman, E., Class, H.: Porosity-permeability relations for evolving pore space: A review with a focus on (bio-)geochemically altered porous media. Transport in Porous Media **124**(2), 589–629 (2018). DOI 10.1007/s11242-018-1086-2. URL https://doi.org/10.1007/s11242-018-1086-2
22. Hornung, U., Jäger, W., Mikelić, A.: Reactive transport through an array of cells with semi-permeable membranes. ESAIM: Mathematical Modelling and Numerical Analysis - Modélisation Mathématique et Analyse Numérique **28**(1), 59–94 (1994)
23. Jaffré, J., Mnejja, M., Roberts, J.E.: A discrete fracture model for two-phase flow with matrix-fracture interaction. Procedia Computer Science **4**, 967–973 (2011). DOI 10.1016/j.procs.2011.04.102. URL http://www.sciencedirect.com/science/article/pii/S1877050911001608
24. Katz, G.E., Berkowitz, B., Guadagnini, A., Saaltink, M.W.: Experimental and modeling investigation of multicomponent reactive transport in porous media. Journal of Contaminant Hydrology **120–121**, 27–44 (2011). DOI https://doi.org/10.1016/j.jconhyd.2009.11.002. URL http://www.sciencedirect.com/science/article/pii/S0169772209001582. Reactive Transport in the Subsurface: Mixing, Spreading and Reaction in Heterogeneous Media
25. Knabner, P., van Duijn, C., Hengst, S.: An analysis of crystal dissolution fronts in flows through porous media. part 1: Compatible boundary conditions. Advances in Water Resources **18**(3), 171–185 (1995). DOI https://doi.org/10.1016/0309-1708(95)00005-4. URL http://www.sciencedirect.com/science/article/pii/0309170895000054
26. Kumar, K., van Noorden, T.L., Pop, I.S.: Effective dispersion equations for reactive flows involving free boundaries at the microscale. Multiscale Modeling & Simulation **9**(1), 29–58 (2011). DOI 10.1137/100804553. URL https://doi.org/10.1137/100804553
27. Martin, V., Jaffré, J., Roberts, J.E.: Modeling Fractures and Barriers as Interfaces for Flow in Porous Media. SIAM J. Sci. Comput. **26**(5), 1667–1691 (2005). DOI 10.1137/S1064827503429363
28. van Noorden, T.: Crystal precipitation and dissolution in a thin strip. European Journal of Applied Mathematics **20**(1), 69–91 (2009). DOI 10.1017/S0956792508007651
29. van Noorden, T.L.: Crystal precipitation and dissolution in a porous medium: Effective equations and numerical experiments. Multiscale Modeling & Simulation **7**(3), 1220–1236 (2009). DOI 10.1137/080722096. URL https://doi.org/10.1137/080722096
30. Ray, N., Oberlander, J., Frolkovic, P.: Numerical investigation of a fully coupled micro-macro model for mineral dissolution and precipitation. Computational Geosciences **23**(5), 1173–1192 (2019). DOI 10.1007/s10596-019-09876-x. URL https://doi.org/10.1007/s10596-019-09876-x
31. Sandve, T.H., Berre, I., Nordbotten, J.M.: An efficient multi-point flux approximation method for Discrete Fracture-Matrix simulations. Journal of Computational Physics **231**(9), 3784–3800 (2012). DOI https://doi.org/10.1016/j.jcp.2012.01.023. URL http://www.sciencedirect.com/science/article/pii/S0021999112000447

315 32. Schwenck, N., Flemisch, B., Helmig, R., Wohlmuth, B.: Dimensionally reduced flow models in fractured porous media: crossings and boundaries. Computational Geosciences **19**(6), 1219–1230 (2015). DOI 10.1007/s10596-015-9536-1. URL http://dx.doi.org/10.1007/s10596-015-9536-1
33. Scotti, A., Formaggia, L., Sottocasa, F.: Analysis of a mimetic finite difference ap-
320 proximation of flows in fractured porous media. ESAIM: M2AN (2017). DOI doi.org/10.1051/m2an/2017028
34. Stefansson, I., Berre, I., Keilegavlen, E.: Finite-volume discretisations for flow in fractured porous media. Transport in Porous Media **124**(2), 439–462 (2018). DOI 10.1007/s11242-018-1077-3. URL https://doi.org/10.1007/s11242-018-1077-3
325 35. Ucar, E., Keilegavlen, E., Berre, I., Nordbotten, J.M.: A finite-volume discretization for deformation of fractured media. Computational Geosciences **22**(4), 993–1007 (2018). DOI 10.1007/s10596-018-9734-8. URL https://doi.org/10.1007/s10596-018-9734-8

MOX Technical Reports, last issues

Dipartimento di Matematica
Politecnico di Milano, Via Bonardi 9 - 20133 Milano (Italy)

06/2020 Domanin, M.; Piazzoli, G.; Trimarchi, S.; Vergara, C.
Image-based displacements analysis and computational blood dynamics after endovascular aneurysm repair

04/2020 Didkovskyi, O.; Azzone, G.; Menafoglio A.; Secchi P.
Social and material vulnerability in the face of seismic hazard: an analysis of the Italian case

05/2020 Artioli, E.; Beiraoda Veiga, L.; Verani, M.
An adaptive curved virtual element method for the statistical homogenization of random fibre-reinforced composites

02/2020 Fresca, S.; Dede', L.; Manzoni, A.
A comprehensive deep learning-based approach to reduced order modeling of nonlinear time-dependent parametrized PDEs

03/2020 Ferro, N.; Micheletti, S.; Perotto, S.
Compliance-stress constrained mass minimization for topology optimization on anisotropic meshes

01/2020 Pozzi, S.; Vergara, C.
Mathematical and numerical models of atherosclerotic plaque progression in carotid arteries

57/2019 Antonietti, P.F.; Bertoluzza, S.; Prada, D.; Verani M.
The Virtual Element Method for a Minimal Surface Problem

60/2019 Ieva, F; Paganoni, A.M.; Romo, J.; Tarabelloni, N.
roahd Package: Robust Analysis of High Dimensional Data

58/2019 Antonietti, P.F; Manzini, G.; Mourad, H.M.; Verani, M.
The virtual element method for linear elastodynamics models. Design, analysis, and implementation

56/2019 Antonietti, P.F.; Berrone, S.; Borio A.; D'Auria A.; Verani, M.; Weisser, S.
Anisotropic a posteriori error estimate for the Virtual Element Method